

Cite this: DOI: 00.0000/xxxxxxxxxx

Shear-induced glass-to-crystal transition in anisotropic clay-like suspensions:† supplementary information

Vincent Labalette,^{ab} Alexis Praga,^{ab} Florent Girard,^{ab} Martine Meireles,^a Yannick Hallez,^a and Jeffrey F. Morris^c

Received Date

Accepted Date

DOI: 00.0000/xxxxxxxxxx

To investigate the nature of the different states presented in Fig. 3 of the main article, we used several quantities defined below in the first section. In the rest of the document, these quantities and others are used to characterize the different phases observed in terms of dynamics and local microstructure.

1 Definitions of the computed quantities

The nematic order parameter S_{nem} has already been defined in the paper. It is used to characterize the alignment of the platelets and its temporal evolution is also used to check if an arrested or equilibrium state is reached.

The 1D radial distribution function is computed as

$$g(r) = \frac{1}{4\pi r^2 N_p \rho} \left\langle \sum_{i=1}^{N_p} \sum_{j \neq i}^{N_p} \delta(r - r_{ij}) \right\rangle \quad (1)$$

where the bracket $\langle \cdot \rangle$ denotes an ensemble average, N_p the number of particles, ρ the mean density, r_{ij} the distance between the centers of gravity of particles i and j , and δ the Dirac delta function.

The structure factor is

$$S_L(\mathbf{q}) = \sum_{i=1}^{N_p} \sum_{j=1}^{N_p} \langle \exp[-i\mathbf{q} \cdot \mathbf{r}_{ij}] \rangle \quad (2)$$

where \mathbf{q} stands for the incident scattering vector, $\mathbf{r}_{ij} = \mathbf{r}_j - \mathbf{r}_i$, and the subscript L refers to the system size, *i.e.*, a three dimensional simulation box of length L and volume L^3 . Due to the finite size of the system and its periodicity, the microscopic density is enforced to be a periodic function. Thus, the values of admissible \mathbf{q} must be commensurate with the box length, corresponding to the periodicity of the system¹ and can be defined as:

$$\mathbf{q} = \frac{2\pi}{L} (n_x, n_y, n_z) \quad (3)$$

where n_x , n_y and n_z are any integers. It is important to stress that any vector $\|\mathbf{q}\|$ smaller than $2\pi/L$ is nonphysical. The static struc-

ture factor will often be represented as a function of the modulus $q = \|\mathbf{q}\|$ to provide information concerning the arrangement of percolated structures and glassy states. Due to the relatively small number of particles simulated and the small box size, the function $S_L(q)$ could sometimes appear to be sampled too coarsely at low scattering vector. The only way to improve this is to increase the size of the box.

The incoherent (one particle) part of the intermediate scattering function $F(\mathbf{q}, t, t_w)$ is the time correlation function of the density in the Fourier space:

$$F_L(\mathbf{q}, t, t_w) = \frac{1}{N_p} \sum_{i=1}^{N_p} \langle \exp[-i\mathbf{q} \cdot (\mathbf{r}_i(t + t_w) - \mathbf{r}_i(t_w))] \rangle \quad (4)$$

where t and t_w are respectively the time and the waiting time. The latter corresponds to the aging time at which the intermediate scattering function starts to be computed. This function provides information concerning the dynamic behavior of the particles. The aging time needed experimentally for suspensions of Laponite to reach the ergodic regime varies from hours to months or even years, depending on the volume fraction and the ionic strength. Although we are working at higher concentrations compared to experiments, we do not expect to be able to reach an ergodic state and, therefore, to evaluate the ergodicity breaking time. Despite the fact that our simulations are short compared to experiments, we are able to capture behaviors similar to those obtained experimentally for both gels and glasses by Jabbari and coworkers^{2,3}, Ruzicka et al.^{4,5} and numerically using Brownian dynamics by Mossa and coworkers⁶.

The orientational correlation function is represented by the average of the second Legendre polynomial of the azimuthal angle θ between the normals of two plate-like particles.

$$P_2(r) = \left\langle \frac{1}{2} (3\cos^2 \theta(r) - 1) \right\rangle. \quad (5)$$

where $\theta = \arccos(\mathbf{n}_i \cdot \mathbf{n}_j)$, and \mathbf{n}_i and \mathbf{n}_j are the normal vectors of particles i and j . When $P_2(r) = -1/2$ the particles are perpen-

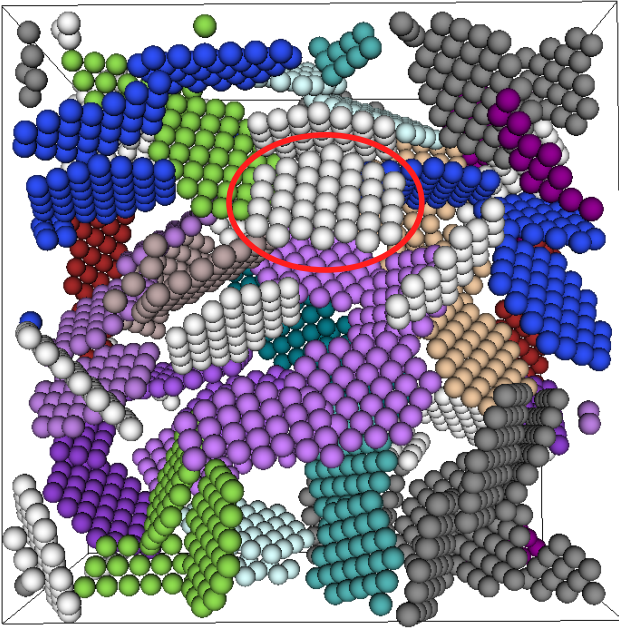


Fig. 1 Example of a snapshot of the microstructure. Each color represents a cluster except for the white color which represents particles without contact (see the particle in the red circle).

dicular while $P_2(r) = 1$ refers to parallel particles. The combination of the radial distribution and orientation pair distribution functions provides a good insight into the microstructure of the system. Nevertheless, these functions do not furnish any information concerning the formation of a gel state, or any percolated structure.

We introduced a criterion of distance to determine when two or more particles are connected and form a cluster: if the gap between two spheres of distinct plate-like particles is less than $0.2a$, where a is the radius of one sphere, the particles are considered in contact. Using this criterion, Figure 1 gives an example of a snapshot where particles belonging to the same cluster will be represented using the same color, as in the main article. A particle without any contact is colored in white, as pointed out by the red circle in Figure 1.

It is also interesting to compute the mean azimuthal angle $\langle \theta \rangle$ defined previously but for touching particles only. This allows investigating the possible correlation between this angle and the position of the contact relative to the center of gravity of the particles. The distance between the contact point in red in Figure 2 and the center of gravity of the particle will be referred to as the "touching distance". This combination of both the angle and the touching distance allows a quite complete insight into the spatial arrangement between particles in contact.

2 Glassy states in region "A" of Fig. 3 in the main article

The simulations reported in region A were run with $\kappa D = 1.46$. At such a long range of interaction, the double layers strongly overlap for the full range of volume fractions investigated here. An analysis of the interaction force between an isolated couple of

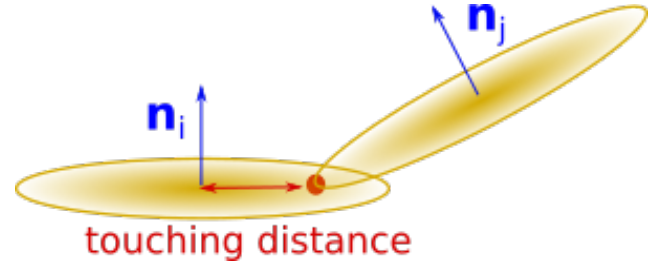


Fig. 2 Definition of the touching distance between two disk-shaped particles. The red point corresponds to the contact point, and the touching distance is defined as the distance between the center of gravity of particle i and the contact point.

platelets at $\kappa D = 1.46$ shows that they are almost always repulsive unless they are nearly touching in overlapping coin configuration.⁷ This strong repulsion is due to the large face charges. At low volume fraction, the system is thus expected to be strongly repulsive. At higher volume fraction, some overlapping coin configurations may be found if platelets can pass the high energy barriers with the help of crowding effects.

Arrested states are often characterized by examining the incoherent intermediate scattering function. In particular, the waiting-time dependence of the non-ergodicity parameter $F(q, \infty, t_w)$ and of the short-time translational diffusion coefficient present marked differences in the glass and gel states.² The incoherent intermediate scattering function is reported in Figure 3 for $\phi = 0.124$, $q = 2\pi/L$ with L the length of the cubic box, and for four different waiting times t_w . The lack of any significant decay on the available time window ($F > 0.96$) clearly shows that the system is arrested. The same dynamical behavior is observed for lower volume fractions but the curves are not reported here. The complete decay of F cannot be observed due to the difficulty to reach very long physical times in the present numerical simulations (the present ASD simulations are devised to resolve hydrodynamic interactions and are thus much slower than Brownian dynamics such as in the study of Mossa and coworkers⁶ for example). Therefore, the ergodicity breaking time and the non-ergodicity parameter cannot be estimated here and F is of limited help.

However, the simulations readily allow us to estimate translational diffusion coefficients at short times D_s at different waiting times from a computation of the mean squared displacements. Jabbari and coworkers² observed that $D_s(t_w)$ remains approximately constant and larger than $0.7D_s(0)$ in glasses. This slowed down but continuously maintained diffusive motion corresponds to the well known "rattling in the cage". In gels, D_s decreases very strongly with t_w and reaches values as low as $0.3D_s(0)$ near the ergodicity breaking time. In this case, the strong reduction of the diffusion coefficient is due to the bonds formed during the percolation of the gel network. The diffusion coefficients corresponding to translations perpendicular and parallel to the platelet director are reported in Figure 4 as a function of the waiting time. For all the volume fractions investigated, they remain above 0.6 at all waiting times in region A, and they do not show any obvious decay. This indicates that the systems in region A of Fig. 3 in the

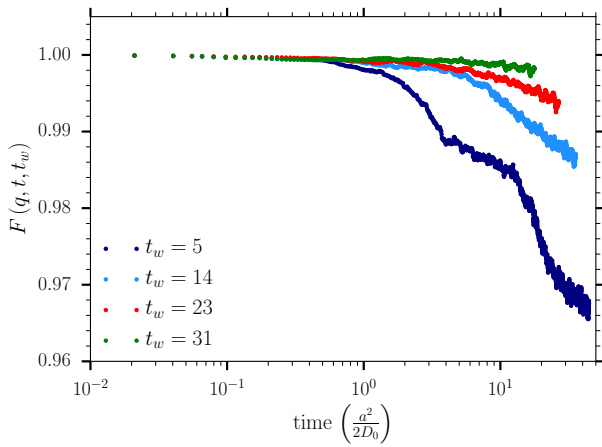


Fig. 3 Incoherent (one particle) intermediate scattering function for $\phi = 0.124$ and $\kappa D = 1.46$. The term t_w stands for the waiting time in non-dimensional time units.

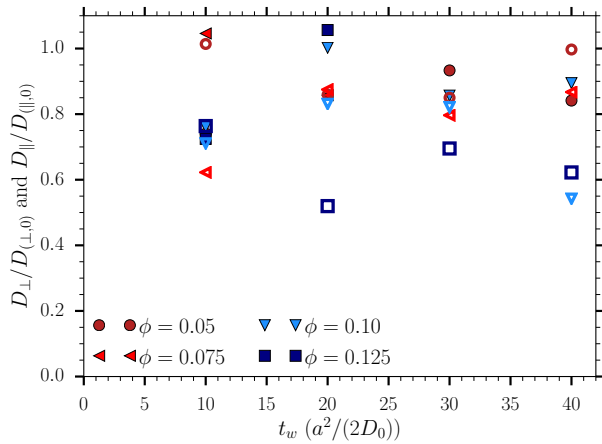


Fig. 4 Evolution of the parallel (empty symbols) and perpendicular (filled symbols) diffusion coefficient normalized to its infinitely dilute value, ($D_{(\perp,0)}$ and $D_{(\parallel,0)}$), at $\kappa D = 1.46$.

main article are glassy.

The osmotic pressure reported in Fig. 5 shows that the suspension is strongly repulsive in region A, at $\kappa D = 1.46$. The static structure factor is reported in Figure 6a for $\phi = 0.05$ and for different time windows, and it is reported in Fig. 6b for other volume fractions and the last time window. It does not evolve with the increase of the "aging" time, in agreement with the assumption of a non-ergodic arrested state within the available simulation time window. The low q behavior confirms that the system has a very low compressibility.

Snapshots in Fig. 7 reveal that among these glass structures, two different final arrested states are observed: a disconnected structure at $\phi = 0.05$ (white platelets are not bonded) and a system highly compressed with structures more and more interconnected as the volume fraction increases. These non-bonded and bonded glasses are identified by the red star and blue triangles in Fig. 3 of the main article, respectively. Let us emphasize that even if the systems at the highest volume fractions do percolate, the

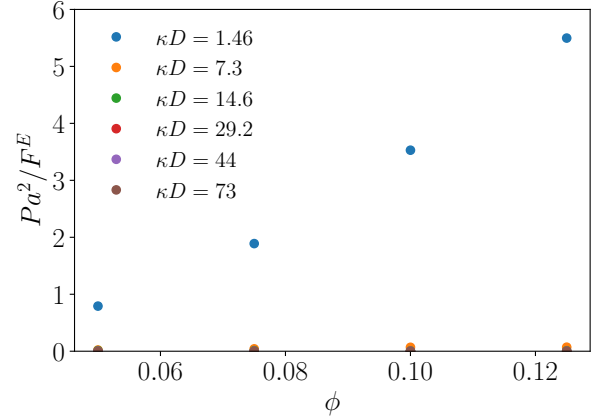
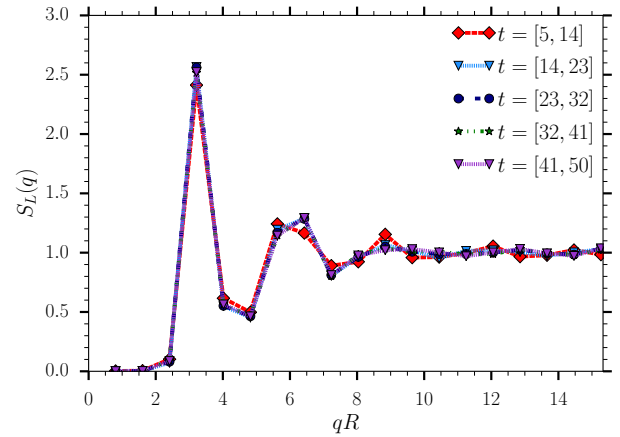
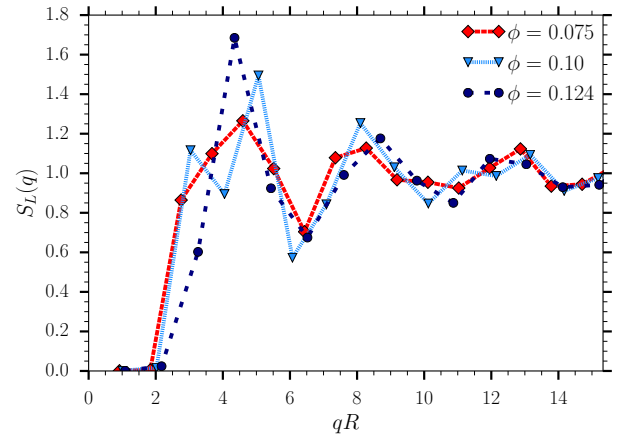


Fig. 5 One component model osmotic pressure computed from eq. (13) in the main article.



(a) For $\phi = 0.05$ and different waiting times.



(b) For $\phi = 0.075, 0.10$ and 0.124 , at the largest waiting time.

Fig. 6 Static structure factors in region A ($\kappa D = 1.46$) and for different waiting times and volume fractions.

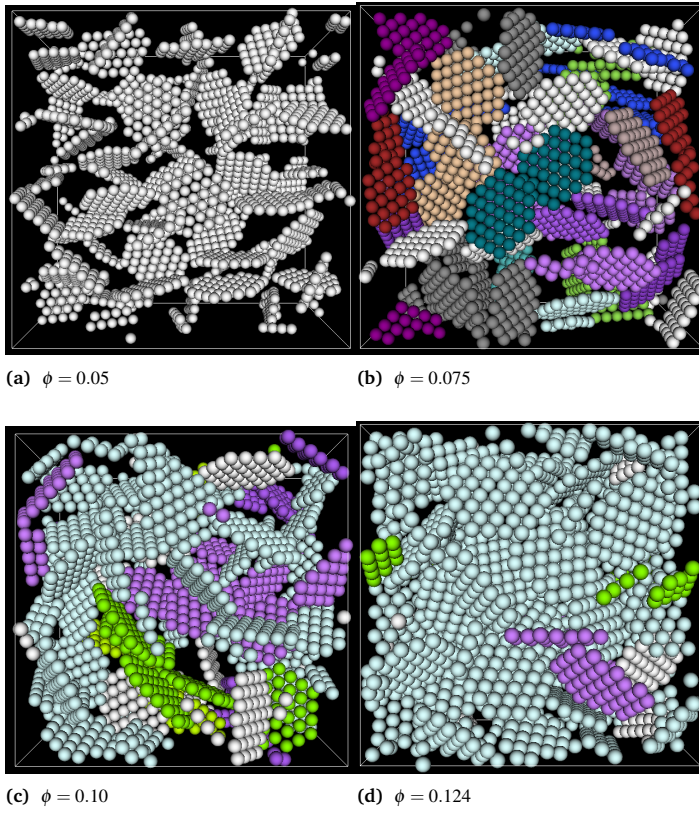
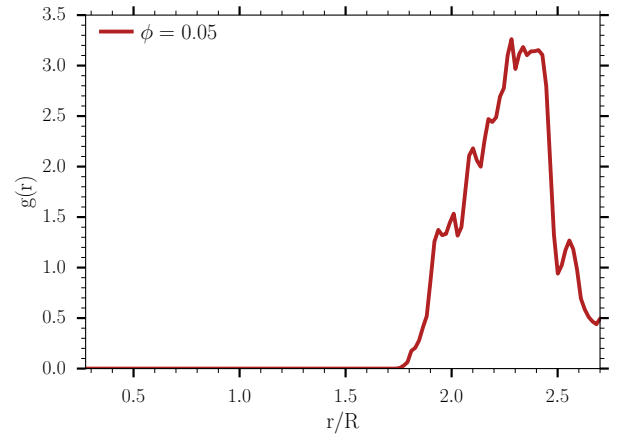


Fig. 7 Snapshot of the microstructure at equilibrium for $\phi = 0.05, 0.075, 0.10$ and 0.124 at $\kappa D = 1.46$.

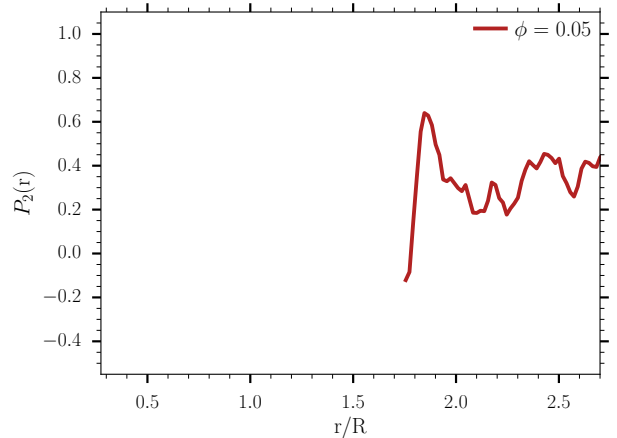
osmotic pressure is very high and they would immediately melt upon dilution. These systems have centers of mass locked in electrostatic cages due to the strong long-range repulsions between faces, but rotational degrees of freedom are used to minimize the global energy by reducing the face-edge distances when possible, leading to these connected structures.

The radial and angular distribution functions presented in Figure 8 provide a good insight into the microstructure of the disconnected glass at $\phi = 0.05$. The primary peak of $g(r)$ is reached between $2.27 R$ and $2.43 R$. Over this range of distance, one can observe in Figure 8b that the orientational correlation function exhibits a kind of plateau at $P_2(r) = 0.43$ indicating that neighboring particles tend to often favor a roughly parallel configuration, although this is far from a truly nematic state.

For volume fractions larger than 0.075 , contacts exist in the glassy phase and the number of connected particles in a "cluster" increases with ϕ (see Fig. 7). Some overlapping coin configurations are observed, especially at the lowest volume fractions (see the two particles in olive color on the center in Figure 7b). In Figure 9a, one can clearly notice that increasing the volume fraction above 0.05 shifts drastically the peak of the radial distribution to lower values. Most of the particles are at a distance equal to $r/R \approx 1.5$ from their neighbors. The intensity of the peak increases and is slightly shifted to lower values with the increase of volume fraction. The radial distribution functions of the particles in contact only (Figure 9b) also exhibit a peak at $1.5R$ but

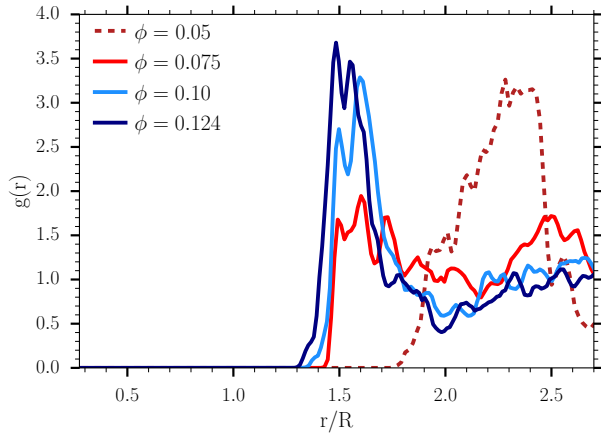


(a) Radial distribution function

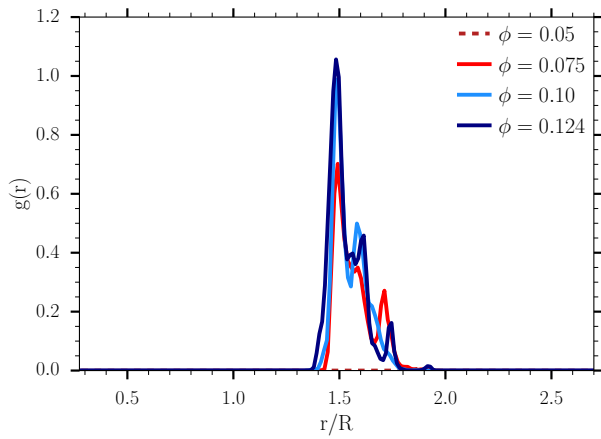


(b) Angular correlation function

Fig. 8 Center of mass radial distribution (left) and second Legendre polynomial function (right) for $\phi = 0.05$ and $\kappa D = 1.46$.



(a) Average over all platelets

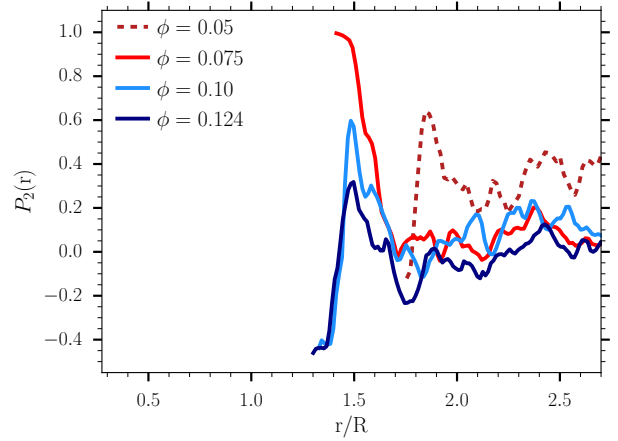


(b) Average over platelets in contact only

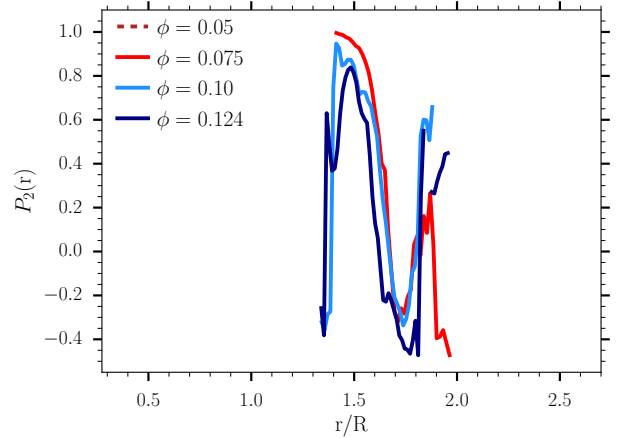
Fig. 9 Center of mass radial distribution functions for long-range electrostatic interactions: $\kappa D = 1.46$.

with an intensity several times lower than that of the $g(r)$ of all particles (see Figure 9a) indicating that only a small fraction of the particles located at this distance are in contact.

The angular correlation functions are reported in Figure 10. In Figure 10a, it can be seen that considering all the particles at the most probable distance of $1.5R$ (in contact or not) P_2 depends strongly on the volume fraction and indicates parallel particles at $\phi = 0.075$ and more or less random orientations for higher concentrations. In contrast, when focusing on particles in contact only (Figure 10b), the large value of P_2 at the same most probable distance indicates parallel particles. Therefore, in these glasses, touching particles are mainly in overlapping coin configuration. Note however that there is a small portion of particles at smaller distances ($1.3R < r < 1.4R$) (Fig. 9a) and that they generally show $P_2 \simeq -0.4$, indicating that some T-shape local configurations also exist.

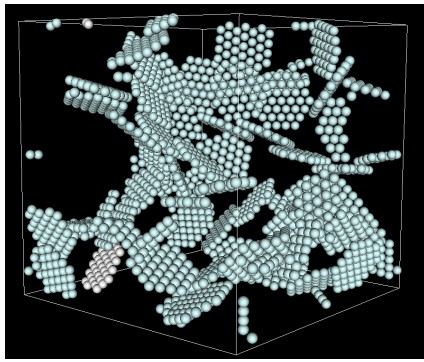


(a) Average over all platelets

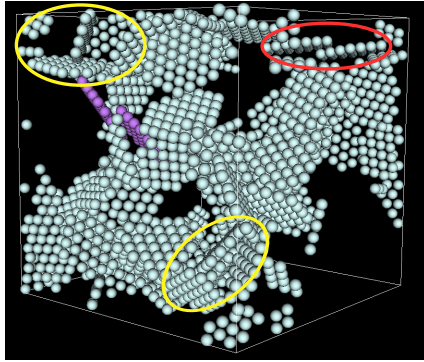


(b) Average over platelets in contact only

Fig. 10 Second Legendre polynomial functions for long-range electrostatic interactions, $\kappa D = 1.46$.



(a) $\phi = 0.05$



(b) $\phi = 0.075$

Fig. 11 Snapshot of the microstructure at equilibrium for $\phi = 0.05$ and $\phi = 0.075$ at intermediate-range electrostatic interactions, $\kappa D = 7.3$. An example of particles in T-shape configuration is circled in yellow and one of particles in OC configuration is circled in red.

3 Aggregated states in regions B and C in the main article.

In regions B and C the interaction range is reduced so the face-rim attractions can compete with face-face repulsions efficiently. This leads to fully or almost fully aggregated states as shown in Fig. 11, with denser zones and large voids in region B. This is typical of gels or phase separating systems.

The structure factors computed at the maximum accessible aging time and $\kappa D = 7.3$ and 14.6 indicate quite compressible systems, with the signature of large scale correlations at the lowest volume fractions (Fig. 12a and 12b). The evolution of $S_L(0)$ with aging time is reported in Fig. 12c and 12d. It increases continuously in time for $\phi = 0.05$ and $\phi = 0.075$ whereas it saturates for higher volume fraction. Such a behavior was also obtained in experiments by Ruzicka and coworkers who observed a phase separation and a static structure factor greater than one at low q for suspensions of Laponite at low volume fraction.⁸ In more concentrated systems, these authors reported an equilibrium gel state with $S_L(0) < 1$.⁹ Regions B and C in Fig. 3 of the main article seem to correspond to these phase separation and an equilibrium gel states, respectively.

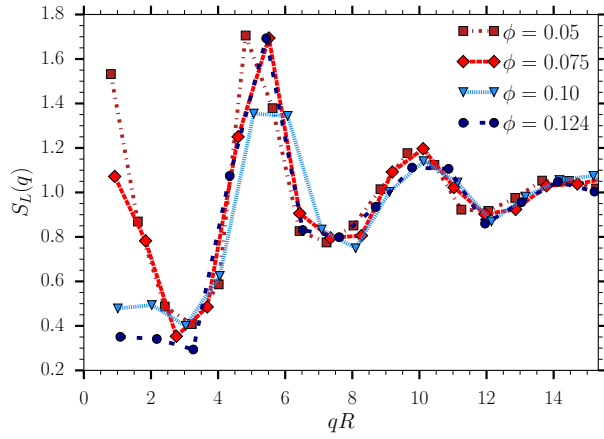
In order to confirm this, the translational diffusion coefficients at short times are reported in Figure 13 for $\kappa D = 14.6$ and for the different volume fractions. They decay globally below 0.6

during the simulation time, in contrast to what was observed for the glassy phase in region A. According to the results of Jabbari-Farouji and co-workers,² this is the behavior of a percolated phase aging with more and more efficient bonds. Thus, the evolution of short time diffusion coefficients with aging time seems to confirm the phase separation process in region B and gel state in region C.

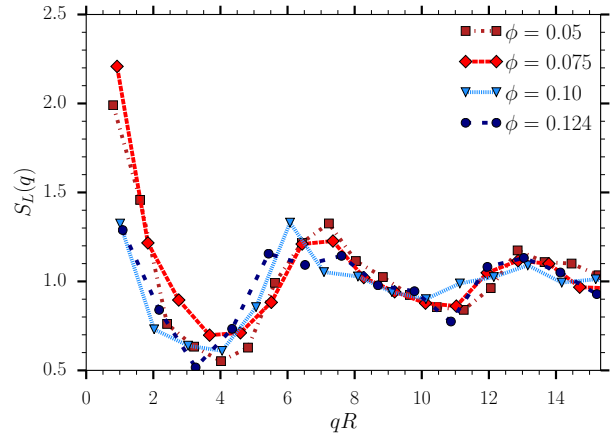
Osmotic pressure values in regions B and C are nearly vanishing for $\kappa D = 7.3$ and oscillate around zero for larger values of κD . (Fig. 5) This is in stark contrast with the very repulsive glassy systems of region A. These vanishing pressures result from the combination of attractive electrostatic interactions and hard-core exclusion forces.

We now turn to the examination of the details of the microstructure at $\kappa D = 7.3$ (red square and green diamonds in Fig. 3 of the main article). The difference in the microstructure between the suspension at $\phi = 0.05$ and suspensions at higher volume fractions is not very clear on the radial distribution function given in Figure 14a. $g(r)$ always exhibits a large peak at a distance of $1.35R$ irrespective of the volume fraction and the system is rather amorphous at larger distances. The angular correlation functions presented in Figure 14b do not help to discriminate between the different structures. A useful indicator is the probability P_θ that two touching particles take a certain angle θ at their contact point. It is represented in Fig. 15 for $\phi = 0.05$ and $\phi = 0.075$. In this figure, the mean distance to contact (cf. section 1) is also reported as $\langle r/R \rangle$, and it does not seem to be correlated to the contact angle. Strikingly, at $\phi = 0.05$, P_θ exhibits a sharp peak for angles from $\theta = 5$ to 12 degrees, which corresponds to the overlapping coin configuration. Then, the probability of having a contact angle $\theta > 20$ degrees slightly decreases up to 45 degrees where two consecutive broad peaks centered at respectively 55 and 78 degrees can be observed. These peaks are only half the intensity of the peak observed at low contact angle, and one can wonder if they are related to the coarse-graining of the particles. The drop of P_θ at 90 degrees indicates that configurations close to a perfect right angle seem almost forbidden. It may be an unstable configuration. At $\phi = 0.075$ (and above), P_θ does not exhibit a dominating peak at low θ values indicating that the OC configuration does exist but is not favored anymore. All contact angles seem to be quite equally likely, so a structure with both overlapping coin and house-of-card arrangements is observed at $\kappa D = 7.3$ and $\phi > 0.075$.

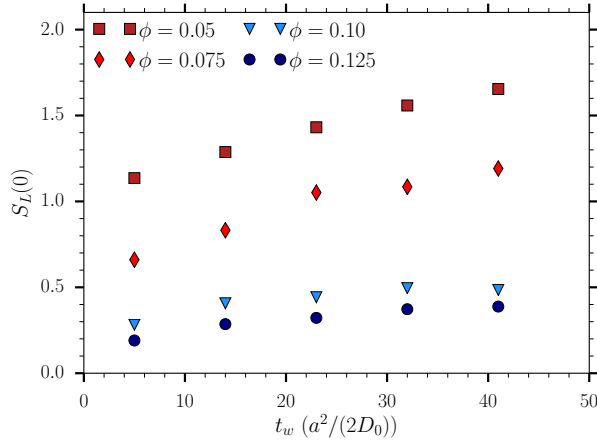
For $\kappa D = 14.6$ and 29.2, the local structure is reported to be dominated by house-of-cards configurations in the main article (purple crosses in Fig. 3). Snapshots are reported in Figure 16. At $\kappa D = 14.6$ and irrespective of the volume fraction, the system is fully percolated, and the particles appear to be in a T-shape configuration. At $\kappa D = 29.2$, isolated clusters and particles appear together with a percolated network for $\phi = 0.05$ and 0.075, while higher volume fractions still generate a fully percolated spanning network. It is possible that the isolated clusters could diffuse and merge with the network for longer simulation times. At $\phi = 0.05$, $g(r)$ exhibits one main peak at $r = R$ for both $\kappa D = 14.6$ and $\kappa D = 29.2$ (see Fig. 17a). At this distance, the corresponding value of the second Legendre polynomial reported in



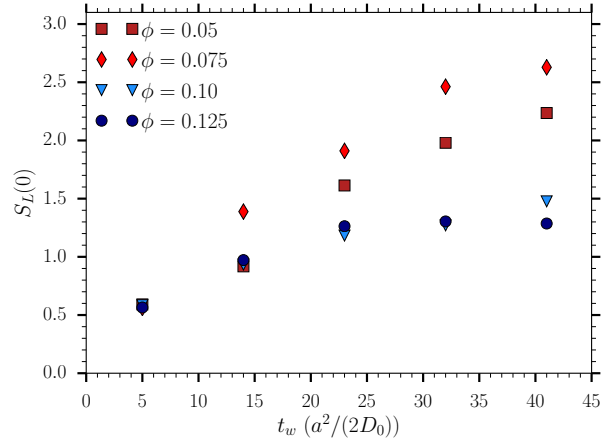
(a) $S_L(q)$ at $\kappa D = 7.3$ and at the end of the simulation.



(b) $S_L(q)$ at $\kappa D = 14.6$ and at the end of the simulation.



(c) $\lim_{q \rightarrow 0} S_L(q)$ at $\kappa D = 7.3$ as a function of the waiting time



(d) $\lim_{q \rightarrow 0} S_L(q)$ at $\kappa D = 14.6$ as a function of the waiting time

Fig. 12 Static structure factor at $\kappa D = 7.3, 14.6$, different volume fractions and aging times.

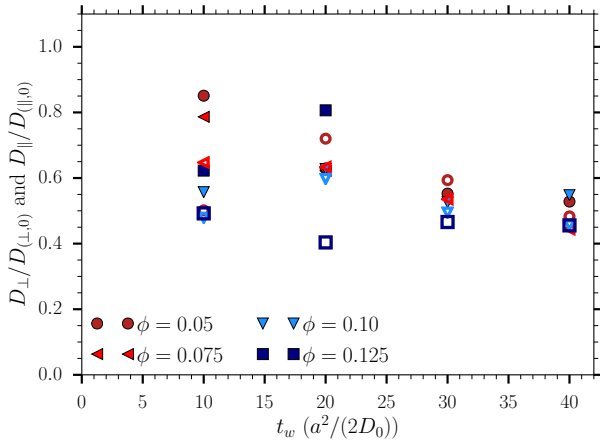
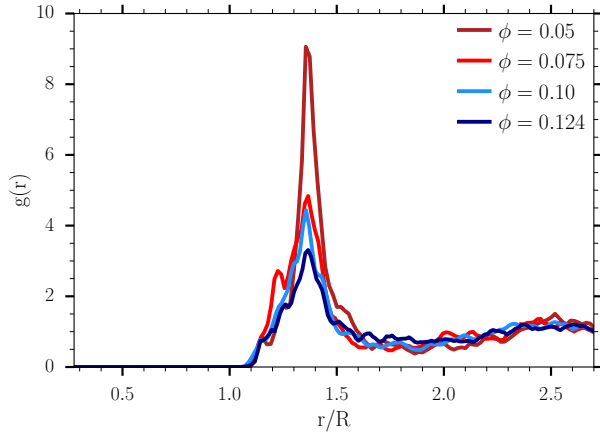
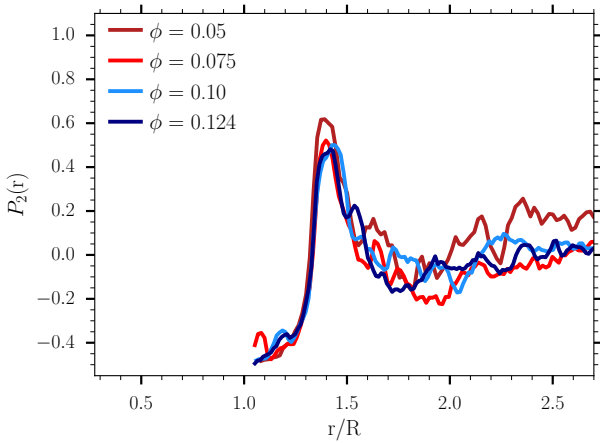


Fig. 13 Translational diffusion coefficients for $\kappa D = 14.6$.

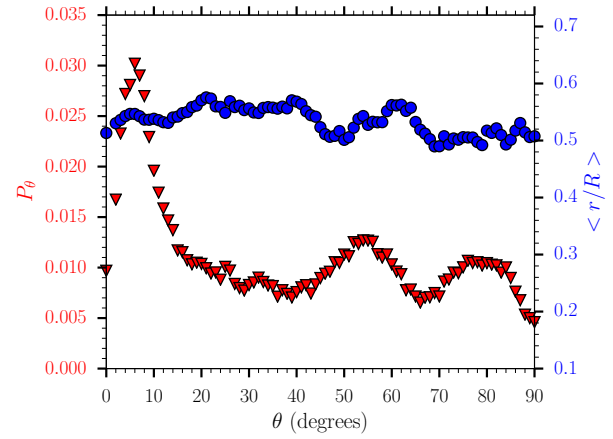


(a) Radial distribution function

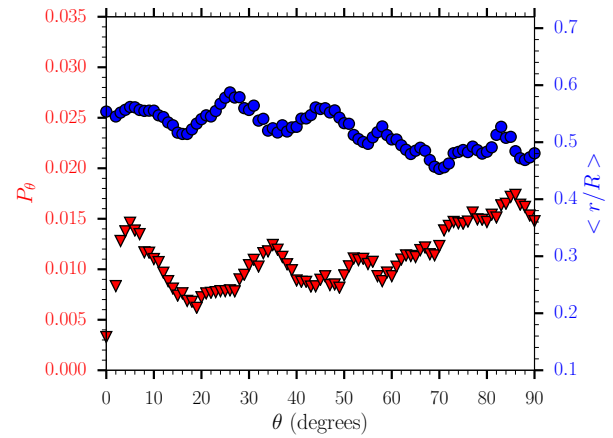


(b) Angular correlation function

Fig. 14 (a) Center of mass radial distribution and (b) second Legendre polynomial function 14b for intermediate range of electrostatic interactions.

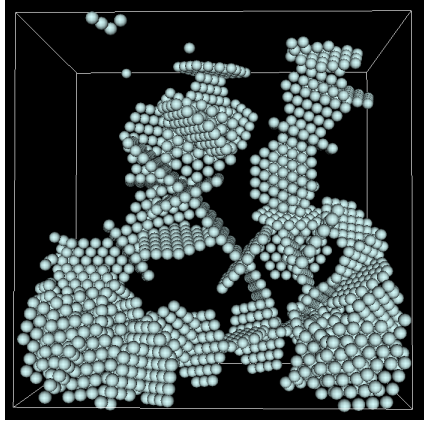


(a) $\phi = 0.05$

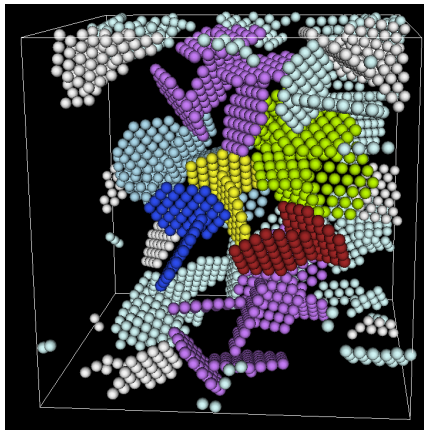


(b) $\phi = 0.075$

Fig. 15 Angle probability P_θ and mean distance to contact $\langle r/R \rangle$ for $\kappa D = 7.3$.



(a) $\kappa D = 14.6$



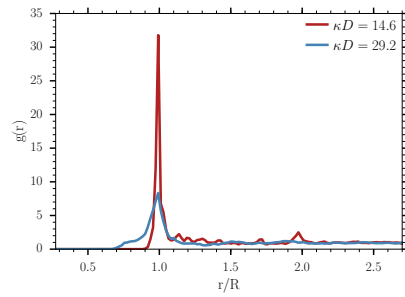
(b) $\kappa D = 29.2$

Fig. 16 Snapshot of the final microstructure obtained for $\phi = 0.05$ and intermediate-range electrostatic interactions.

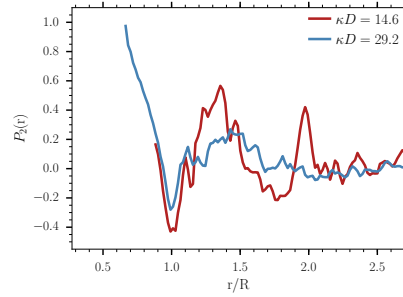
Figure 17b is -0.4 , which indicates that particles are in a T-shape configuration. Note the absence of a peak at $r/R \approx 1.35$ of the radial distribution function, corresponding to the specific distance of the OC configuration observed earlier for longer interaction ranges. The radial distribution function exhibits a small second peak at $2R$ corresponding to the second neighbor in a chain of particles in a T-shape configuration, which is corroborated by the peak on $P_2(r)$ at that same distance. To conclude, at $\phi = 0.05$ and $\kappa D = 14.6$ particles are mostly in the T-shape configuration. The probability of the angle between particles in contact shows a similar behavior for $\kappa D = 14.6$ and $\kappa D = 29.2$ (Fig. 18): no angle below 20° is found and 90° configurations are favored. The corresponding mean distance to contact is close to zero, which is exactly the signature of T-shaped configurations. This T-shape configuration is actually an energy minimum⁷, and as the energy trap is weaker at $\kappa D = 29.2$ than at $\kappa D = 14.6$, one can understand that more configurations can be explored around the 90° configuration at $\kappa D = 29.2$. For increasing volume fractions, the same general picture can be observed (see Fig. 17). The only noticeable evolution is the decrease of the amplitude of the main peak in $g(r)$ with increasing volume fraction and the disappearance of the secondary peak at $r = 2R$. This is due to crowding effects preventing more and more platelets from reaching the favored 90° configuration. To summarize, at $\kappa D = 14.6$ and 29.2 the house-of-cards configuration with an angle close to 90 degrees is preferred to configurations with smaller angles. However, finite volume fraction effects sometimes prevent particles from forming local arrangements with the lowest free energy so angles lower than 90° are progressively more observed with increasing ϕ . The overlapping coin configuration is not favored at these interaction ranges. Hence the house-of-cards configuration has been observed at all volume fractions, with a phase separation below $\phi = 0.08$ and a gel above. These results are in line with Delhomme and coworkers¹⁰ and Ruzicka et al.⁹.

4 Liquid state in region "D" in the main article

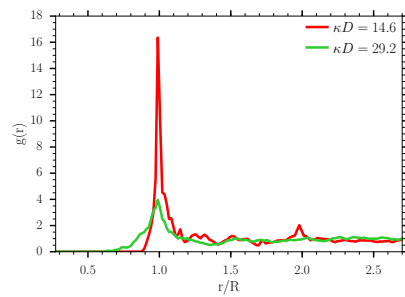
When reducing even more the range of electrostatic interactions, *i.e.*, $\kappa D = 44$ and $\kappa D = 73$, the ratio between the attraction forces and the Brownian forces is not high enough to allow the formation of permanent clusters (platelets appear in white, *i.e.* non-bonded, on the snapshot in Fig. 3g in the main article). This state was described by Ruzicka and coworkers⁹ and was placed above the percolation line, in the liquid phase. The radial distribution function is reported for $\phi = 0.05$ in Fig. 19: it is very close to 1, very noisy due to the lack of converged statistics in this strongly fluctuating system, and the difference between structures with electrostatic interactions and without them ($\kappa D = \infty$) is not obvious. In this liquid phase at extremely short interaction range the suspension behaves as a suspension of Brownian hard platelets. Note that in practice, and as emphasized by Jönsson and coworkers¹¹, van der Waals interactions not included here will play an important role in such high salt conditions so a more detailed study of our results in this liquid phase is of very limited interest.



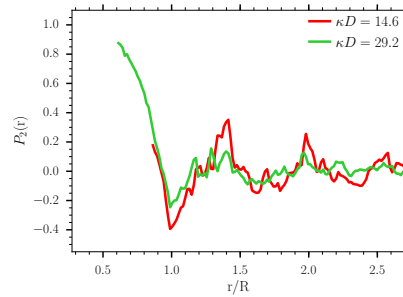
(a) Radial distribution function at $\phi = 0.05$



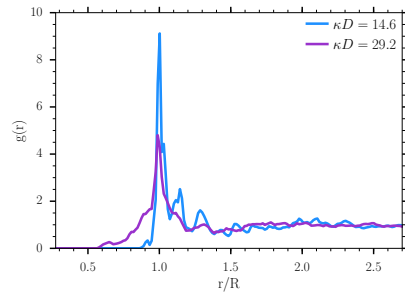
(b) Angular correlation function at $\phi = 0.05$



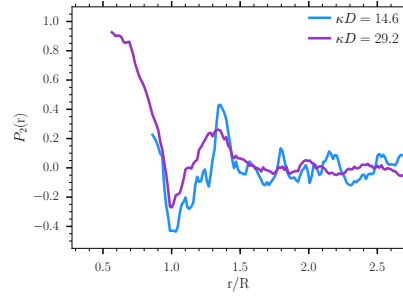
(c) Radial distribution function at $\phi = 0.075$



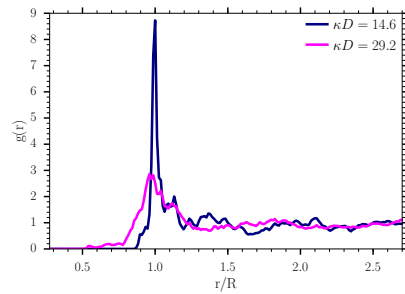
(d) Angular correlation function at $\phi = 0.075$



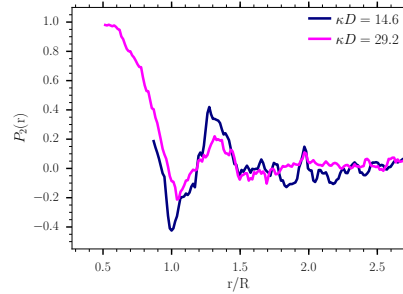
(e) Radial distribution function at $\phi = 0.10$



(f) Angular correlation function at $\phi = 0.10$

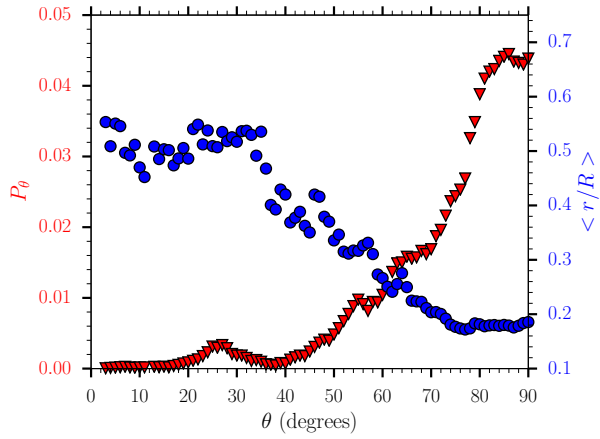


(g) Radial distribution function at $\phi = 0.124$

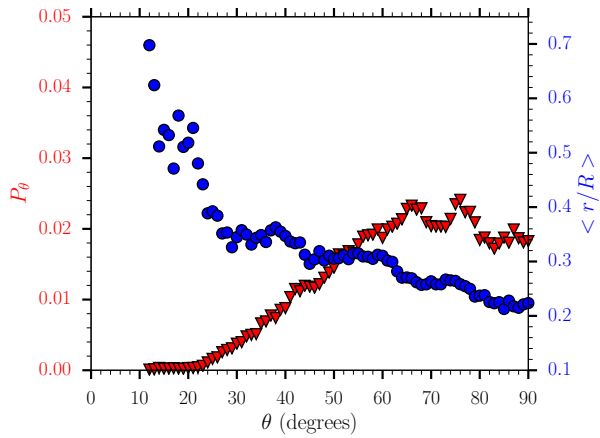


(h) Angular correlation function at $\phi = 0.124$

Fig. 17 Radial distribution function and angle correlation for $\kappa D = 14.6$ and 29.2 .

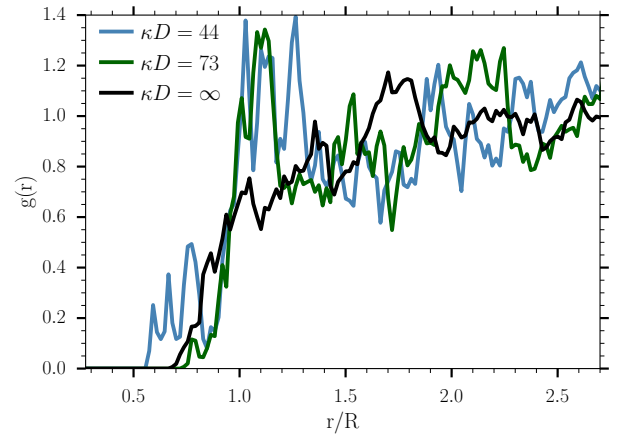


(a) $\kappa D = 14.6$

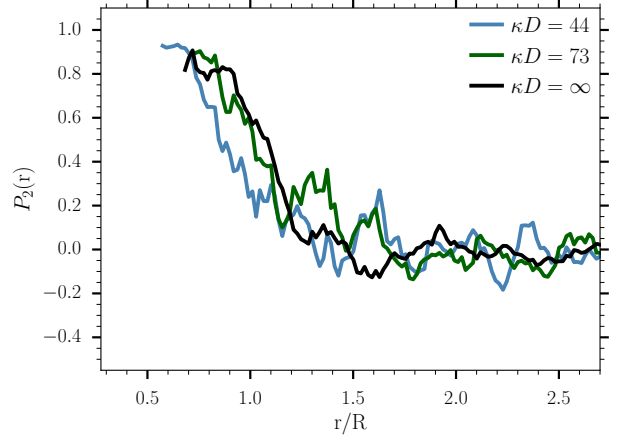


(b) $\kappa D = 29.2$

Fig. 18 Angle probability P_θ and mean distance to contact $\langle r/R \rangle$ at $\phi = 0.05$ for $\kappa D = 14.6$ and $\kappa D = 29.2$.



(a) Radial distribution function



(b) Angular correlation function

Fig. 19 Radial distribution and angular correlation functions at $\phi = 0.05$ for very short-range interactions. The black line stands for hard disks.

Notes and references

- 1 D. Villamaina and E. Trizac, *Eur. J. Phys.*, 2014, **35**, 035011.
- 2 S. Jabbari-Farouji, G. H. Wegdam and D. Bonn, *Physical Review Letters*, 2007, **99**, 065701.
- 3 S. Jabbari-Farouji, H. Tanaka, G. H. Wegdam and D. Bonn, *Physical Review E*, 2008, **78**, 061405.
- 4 B. Ruzicka, L. Zulian and G. Ruocco, *Langmuir*, 2006, **22**, 1106–1111.
- 5 B. Abou, D. Bonn and J. Meunier, *Journal of Rheology*, 2003, **47**, 979–988.
- 6 S. Mossa, C. De Michele and F. Sciortino, *The Journal of Chemical Physics*, 2007, **126**, 014905.
- 7 V. Labalette, *PhD thesis*, Université de Toulouse, Institut National Polytechnique de Toulouse, 2020.
- 8 B. Ruzicka, L. Zulian, E. Zaccarelli, R. Angelini, M. Sztucki, A. MoussaĀrd and G. Ruocco, *Physical Review Letters*, 2010, **104**, 085701.
- 9 B. Ruzicka, E. Zaccarelli, L. Zulian, R. Angelini, M. Sztucki, A. MoussaĀrd, T. Narayanan and F. Sciortino, *Nature Materials*, 2011, **10**, 56–60.
- 10 M. Delhorme, B. JĀúnsson and C. Labbez, *Soft Matter*, 2012, **8**, 9691.
- 11 B. JĀúnsson, C. Labbez and B. Cabane, *Langmuir*, 2008, **24**, 11406–11413.